Available online at www.sciencedirect.com

jmr&t Journal of Materials Research and Technology

journal homepage: www.elsevier.com/locate/jmrt

Original Article

Reinforcement of polystyrene using edge-styrene graphitic nanoplatelets

Yeong A Kang [a,1], Min Hui Kim [a,1], Hyuk-Jun Noh [b], Jong-Beom Baek [b,**], In-Yup Jeon [a,*]

[a] Department of Chemical Engineering, Wonkwang University, 460 Iksandae-ro, Iksan, Jeonbuk, 54538, Republic of Korea

[b] School of Energy and Chemical Engineering/Center for Dimension-Controllable Organic Frameworks, Ulsan National Institute of Science and Technology (UNIST), UNIST-gil 50, Ulsan, 44919, Republic of Korea

ARTICLE INFO

Article history:
Received 13 August 2020
Accepted 11 December 2020
Available online 24 December 2020

Keywords:
Graphitic nanoplatelets
Styrene-graft
Mechanochemical reaction
Compatibility
Polystyrene

ABSTRACT

Edge-styrene graphitic nanoplatelets (StGnPs) were prepared by the *in-situ* mechanochemical reaction between graphite and styrene without additional chemical reaction (*e.g.* functionalization). The resultant StGnPs exhibited excellent properties including good dispersibility in organic solvents, to use an efficient reinforcing additive for polystyrene (PS) that is one of the most widely used plastics. StGnP/PS nanocomposites were prepared easily *via* a facile solution process method. Compared to pure PS, the StGnP/PS nanocomposites exhibited significantly enhanced mechanical properties (*e.g.*, tensile strength, yield strength, Young's modulus, and tensile toughness) along with improved thermal stability. The StGnP/PS nanocomposites showed efficient load transfer from the PS matrix to the StGnPs because of the good dispersibility and compatibility of the StGnPs in the PS matrix. And also, the mechanochemical reaction showed that GnPs having remarkable compatibility of various polymers can be produced freely.

1. Introduction

Carbon-based nanomaterials exhibit attractive properties, and hence are used extensively for various applications [1]. Among these, two-dimensional graphene, which is a single layer of sp^2-hybrid carbon network, has gained significant attention owing to its exceptional mechanical, thermal, and electrical properties [2–4]. Graphene has been extensively investigated as a reinforcing additive to polymers such as polyethylene (PE) [5–7], polypropylene (PP) [8–10], polyvinyl chloride (PVC) [11,12], polystyrene (PS) [13–15], polymethylmethacrylate (PMMA) [16,17], polyurethane (PU) [18,19], nylon [20,21], and epoxy resin [22].

However, scalable and cost-effective production of high-quality graphene is important for its widespread commercial applications. The most commonly used scalable method for

* Corresponding author.
** Corresponding author.
E-mail addresses: jbbaek@unist.ac.kr (J.-B. Baek), iyjeon79@wku.ac.kr (I.-Y. Jeon).
[1] These authors contributed equally.

https://doi.org/10.1016/j.jmrt.2020.12.039

the synthesis of graphene is the chemical oxidation of graphite into graphite oxide, which is then dispersed to form graphene oxide (GO). After solution processing, GO is chemically and/or thermally converted into reduced graphene oxide (rGO). Both GO and rGO contain topological defects (holes) and a large number of oxygenated functional groups (chemical defects) such as epoxy, hydroxyl, and carboxyl groups on both the graphitic basal plane and edges [23–25]. These physical and chemical defects deteriorate the graphitic structure and properties of graphene. Furthermore, bulk GO and rGO exhibit particle agglomeration owing to their high surface energy (*e.g.*, polar interaction and van der Waals forces). GO and rGO are not effective reinforcing additives for GO (and rGO)/polymer nanocomposites [26]. Therefore, high-quality carbon-based nanomaterials with good solvent and/or polymer matrix dispersibility are suitable for application as reinforcing additives in carbon-based polymer nanocomposites. Hence, in order to render graphitic materials suitable for reinforcing polymer composites, their tedious post-functionalization is necessary to achieve stable dispersions in solvents or the polymer matrix [27–29]. For example, alkyl-functionalized GO or rGO showed good dispersibility in non-polar organic solvents and polymers [30,31]. Hence, the developing a method to synthesize high-quality graphitic materials with good solvent dispersibility is very important.

In this study, we developed a one-step scalable method to produce graphitic nanoplatelets (GnPs) at low cost using a mechanochemistry [32–34]. Edge-styrene graphitic nanoplatelets (StGnPs) were prepared directly by ball-milling graphite in the presence of styrene without additional chemical reaction. The StGnPs showed good chemical affinity (good compatibility) to PS because of the presence of styrene moieties at the edge of GnPs. Indeed, the StGnPs were well-dispersible in organic solvents, especially, tetrahydrofuran (THF). StGnP/PS nanocomposites were prepared easily *via* solution processing method and these nanocomposites exhibited considerably improved mechanical properties (*e.g.* the tensile strength, yield strength, Young's modulus, and tensile toughness) compared to pure PS.

2. Experimental

2.1. Materials

Graphite was obtained from Alfa Aesar (Natural, −100 mesh, 99.9995% metals basis) used as received. Styrene (≥99%) was purchased from Aldrich Chemical Inc. and used after removing the stabilizer by using glass filter. All other solvents were supplied by Aldrich Chemical Inc. and used without further purification, unless otherwise specified.

2.2. Preparation of StGnPs

StGnPs were made *in-situ* from graphite and styrene by ball-milling approach. Graphite (5.0 g) and styrene (10 ml) without the stabilizer were placed into a stainless steel reactor with stainless steel balls (500 g, diameter 5 mm). After assembling reactor, the pump sucks air out through the valve. The reactor was fixed in the planetary ball-mill, and then spun at 500 rpm for 48h. After reaction, the product was treated with 1 M aq. HCl to remove metallic impurities and further eliminated clearly unreacted styrene *via* Soxhlet extractor with acetone. Finally, the product, StGnPs, was freeze-dried at −120 °C under a reduced pressure (0.05 mmHg) for 48h to yield 9.14 g (styrene content at least 4.14 g) of dark black powder.

2.3. Sulfonation of StGnPs

Chlorosulfonic acid (99%, 30 mL) was slowly added into the StGnPs (1.0 g) and stirred without heating in the flask. After 12 h, the resultant product was poured into distilled water. It was collected by filtration and further Soxhlet extracted with distilled water to remove impurities. Final product was then freeze-dried at −120 °C under a reduced pressure (0.05 mmHg) for 48h to yield 1.11 g. Found: C, 73.69%; H, 2.40%; S, 2.07%; O, 18.34%.

2.4. Preparation of StGnP/PS nanocomposites

StGnP/PS nanocomposites were prepared by using solution mixing method. To make StGnP/THF solution, the StGnPs were dispersive in THF by using tip-sonication for 1 h. And also, PS were soluble in THF at room temperature. To make StGnP/PS/THF solution, StGnP/THF solution was dropped into PS/THF solution. The mixed solution was stirred for 24 h. StGnP/PS/THF solution was poured slowly into glass petri dish. THF was removed very slowly at 40 °C (24 h), 50 °C (24 h) and 60 °C (24 h). Finally, the resultant nanocomposites were dried clearly under reduced pressure (0.5 mmHg) at 70 °C for 24 h. The contents of the StGnPs into StGnP/PS nanocomposites were 0, 1, 2, 5, and 10 wt.%, respectively. To measure mechanical properties of the pure PS and StGnP/PS nanocomposite, we obtain a nanocomposite board that can be cut into dumbbell-shaped test samples with the dimensions of 79.5 mm × 4.3 mm × 0.23 mm (L × W × T).

2.5. Instrumentations

Elemental analysis (EA) was conducted with Thermo Scientific Flash 2000. The field emission scanning electron microscopy (FE-SEM) was performed on FEI Nanonova 230. The surface area was measured by nitrogen adsorption–desorption isotherms using the Brunauer–Emmett–Teller (BET) method on Micromeritics ASAP 2504N. X-ray photoelectron spectra (XPS) were recorded on a Thermo Fisher K-alpha XPS spectrometer. Themogravimetric analysis (TGA) was conducted on a TA Q200 (TA Instrument) under air and nitrogen at a heating rate of 10 °C min^{-1}. Differential scanning calorimetry (DSC) experiments were carried out using a DSC4000 (PerkinElmer) at a heating rate of 10 °C min^{-1} and same cooling rate. X-Ray diffraction (XRD) patterns were recorded with a Rigaku D/MAZX 2500V/PC with Cu0Kα radiation (35 kV, 20 mA, $\lambda = 1.5418$ Å). The tensile properties of raw PS and StGnP/PS nanocomposites were measured at room temperature on a universal testing machine, DR101 (DRTECH Co., Korea) at a strain rate of 100 mm min^{-1}.

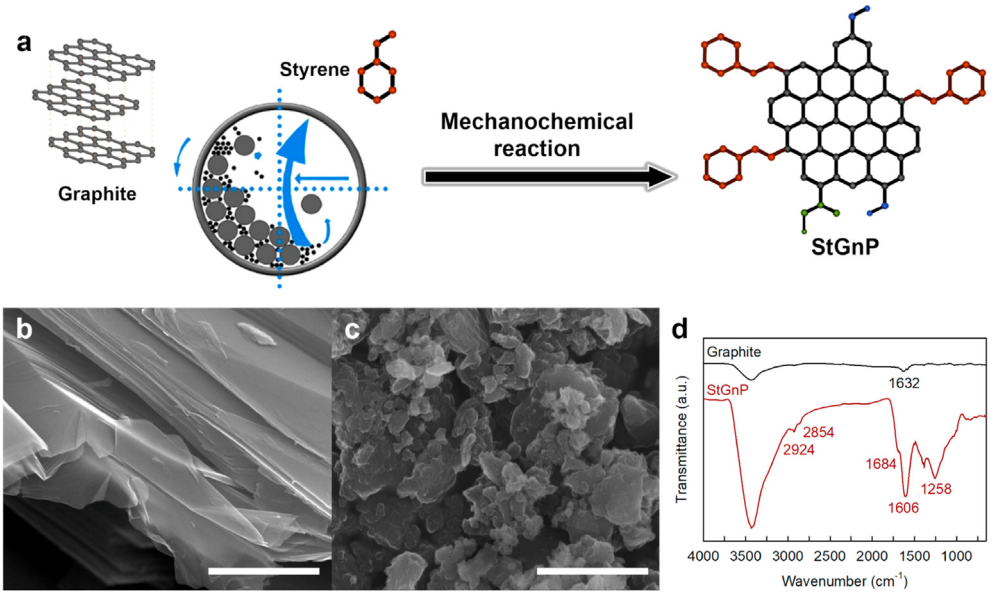

Fig. 1 – (a) Schematic for the direct preparation of the StGnPs *via* a mechanochemical reaction. SEM images: (b) the pristine graphite; (c) StGnPs. Scale bars are 1 μm. (d) FT-IR spectra of the pristine graphite and the StGnPs.

3. Results and discussion

Edge-styrene graphitic nanoplatelets (StGnPs) were prepared directly *via* a mechanochemical reaction between graphite (<100 mesh) and styrene without additional chemical reaction (Experimental details are described in Supplementary Information) (Fig. 1a). Before carrying out the reaction, the inhibitor in styrene was removed. The StGnPs obtained after the reaction were washed thoroughly with a 1 M aq. HCl solution to remove the pulverized metal impurities present in them. The unreacted styrene was completely removed by Soxhlet extraction with acetone.

The morphologies of the samples before and after ball-milling were examined by using field-emission scanning electron microscopy (FE-SEM). The SEM image of the pristine graphite showed thick layered flakes with a large grain size (<150 μm) and sharp edges (Fig. 1b), while the StGnPs showed small spherical particles with a dramatically reduced grain size (<1 μm) and smooth edges. The morphology of the StGnPs was similar to those of previously reported GnPs (Figs. S1c and S1) [32–34]. The tremendous decrease in the grain size of the StGnPs as compared to that of the pristine graphite indicates that the graphitic C–C bonds of graphite unzipped and active carbon species (C•) were generated during the reaction between graphite and styrene to produce the StGnPs. As a result, styrene moieties are attached at the edges of StGnPs as form of monomer and/or oligomers. The SEM energy dispersive X-ray (EDX) spectrum of the StGnPs exhibited only C and O peaks (Fig. S2b). The C and O contents of the StGnPs were found to be 90.05 and 9.95 at.%, respectively (Table S1). The C and O elemental mapping images of the StGnPs are shown in Figs. S2c and S2d, respectively. The presence of oxygen in the StGnPs can be attributed to the physically adsorbed air-moisture [35,36] and oxygenated functional groups (–OH, –COOH, C=O, and so on), which were introduced during the elimination of the remnant active carbon species.

Fourier-transform infrared (FT-IR) spectroscopy is generally used for the qualitative analysis (*e.g.,* the functional groups, isomers, hydrogen bonds, and so on) of organic materials. The FT-IR spectrum of the pristine graphite showed a weak peak at 1632 cm^{-1} corresponding to the vibration mode of the adsorbed water molecules [32,37]. However, the StGnPs showed an intense sp^2 C–H stretch peak at 2924 and sp^3 C–H stretch peak at 2854 cm^{-1} as well as an aromatic C=C stretch peak at 1606 cm^{-1} (Fig. 1d). These peaks confirmed the presence of styrene at the edges of the StGnPs. The StGnPs showed a C=O stretch peak at 1684 cm^{-1} and a C–O stretch peak at 1258 cm^{-1} corresponding to the oxygenated groups introduced during the work-up procedure [32,33,38]. This is consistent with the SEM-EDX results.

To further confirm the grafting of styrene at the edges of the GnPs, the StGnPs were sulfonated with chlorosulfonic acid ($ClSO_3H$), which can be selectively functionalized to the phenyl ring of styrene [39,40]. The S content of the sulfonated StGnPs was approximately 2.07 wt.%, indicating that a large number of styrene units were present at the edges of the StGnPs (Table S1 and Fig. S3).

The chemical compositions and bonding natures of the samples were analyzed using X-ray photoelectron spectroscopy (XPS) (Fig. 2a). The pristine graphite showed an intense C1s peak and a weak O1s peak [41,42]. This result is consistent with the SEM-EDX and FT-IR results [32,33,38]. The C1s peak of the StGnPs could be deconvoluted into three peaks: sp^2 C–C (284.7 eV), C–O (285.7 eV), and C=O (289.0 eV) (Fig. S4a) [43], and the O1s peak could be deconvoluted into two peaks: C=O (532.5 eV) and C–O (533.6 eV) (Fig. S4b) [43].

The specific surface areas (SSAs) of the samples were measured by obtaining their N_2 adsorption/desorption isotherms using the Brunauer–Emmett–Teller (BET) method.

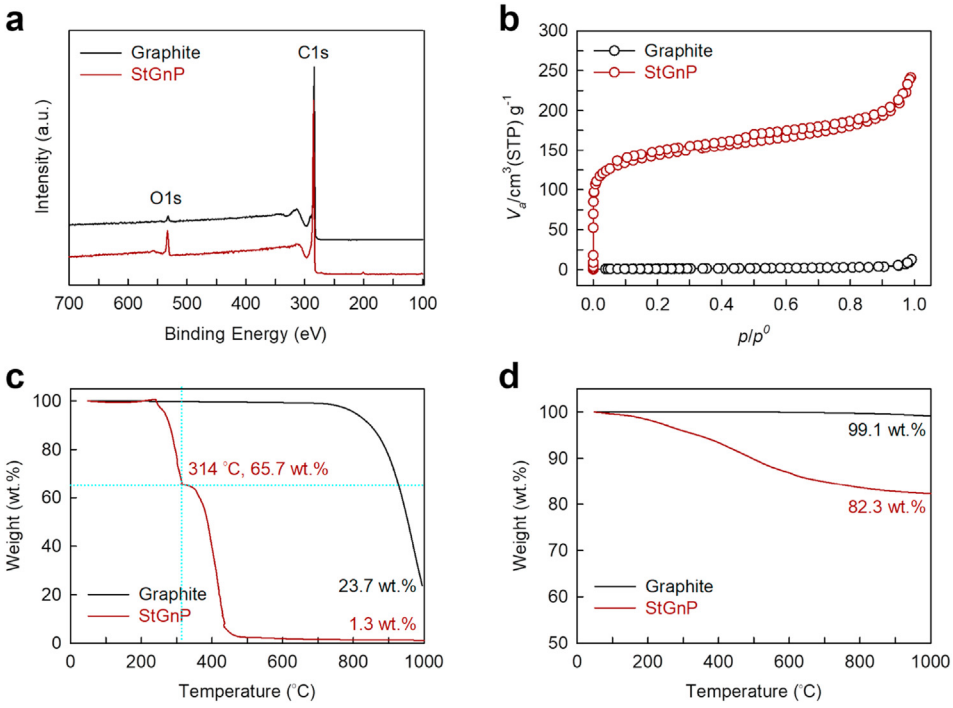

Fig. 2 – (a) XPS survey spectra of the pristine graphite and the StGnPs. (b) N_2-adsorption/desorption isotherms at 77 K of the pristine graphite and the StGnPs. TGA thermograms of the pristine graphite and the StGnPs obtained at the heating rate of 10 °C min^{-1}: (c) in air; (d) in N_2.

The SSAs of the pristine graphite and the StGnPs were 2.78 and 535.69 m^2 g^{-1}, respectively (Table S2). The significantly large surface area (193 times larger than that of the pristine graphite) of the StGnPs indicates that they were delaminated into a few graphitic layers because of the presence of styrene units at the edges. The number of graphitic layers in the StGnPs was estimated to be 4.9 (average) using the theoretical SSA of a single graphene layer (2630 m^2 g^{-1}, 2620/535.69) [44]. Furthermore, the StGnPs showed type-I isotherm and type-H3 hysteresis (P/P° = 0.5–1.0) (Fig. 2b), indicating the presence of micropores and plate-like structure or slit-shaped pores [45]. Thus, when the StGnPs were used as a reinforcing additive to PS, high-performance StGnP/PS nanocomposites were obtained. The enhanced performance of the StGnP/PS nanocomposites can be attributed to the high SSA, edge-styrene grafting, micropores, and plate-like structure of the StGnPs.

The quantitative edge-functionality of the StGnPs was examined by carrying out their thermogravimetric analysis (TGA). The pristine graphite was stable up to 750 °C in air. On the other hand, the StGnPs showed a sharp weight loss of 34.3 wt.% at around 314 °C (Fig. 2c). This can be attributed to the covalently attached edge-functional groups such as styrene and other oxygenated functional groups (*e.g.*, –COOH, –C=O, and –OH) present in the StGnPs. The char yields of the pristine graphite and the StGnPs at 1000 °C in air were 23.7 and 1.3 wt.%, respectively (Fig. 2c). However, their char yields in N_2 were 99.1 and 82.3 wt.%, respectively (Fig. 2d). This indicates that the styrene moieties at the edges of the StGnPs acted as feedstock for C-welding to sustain a high char yield in the presence of nitrogen [46].

The degree of exfoliation of the StGnPs could be further estimated using XRD (Fig. S5). The pristine graphite showed sharp peaks at 2θ = 26.5° (002) and 54.7° (004) corresponding to the C-axis direction perpendicular to the layer planes of graphite [47,48]. However, the StGnPs showed only the peak at 2θ = 26.5° (002). The intensity of the (002) peak in the case of the StGnPs was only 0.7% of that in the case of the pristine graphite. This decrease in the intensity of the (002) peak and the disappearance of the (004) peak in the case of the StGnPs indicate a large extent of exfoliation in the StGnPs. On the basis of the XRD and SSA results, it can be stated that the edge-styrene grafting of the pristine graphite using ball-milling induced the unzipping of graphitic C–C bonds, generating active carbon species (C•), which caused the delamination of the graphitic layers.

The StGnPs showed excellent dispersibility in various solvents such as H_2O, tetrahydrofuran (THF), *N*,*N*-dimethylformamide (DMF), *N*-methyl-2-pyrrolidone (NMP), dichloromethane (CH_2Cl_2), and diethyl ether (Fig. S6). Thus, the StGnPs showed a huge potential to be used as a reinforcing additive to polymer nanocomposites. StGnP/PS nanocomposites could be easily prepared by a solution process in THF and uniform distribution of StGnPs in the PS matrix could be confirmed using high-resolution transmission electron microscopy (HR-TEM, Fig. S7).

Polystyrene (PS) is a widely used thermoplastic and can be easily processed into a large number of semi-finished products including foams, films, and sheets [49,50]. The StGnPs, which showed good compatibility with PS because of their high styrene concentration, were used as a reinforcing

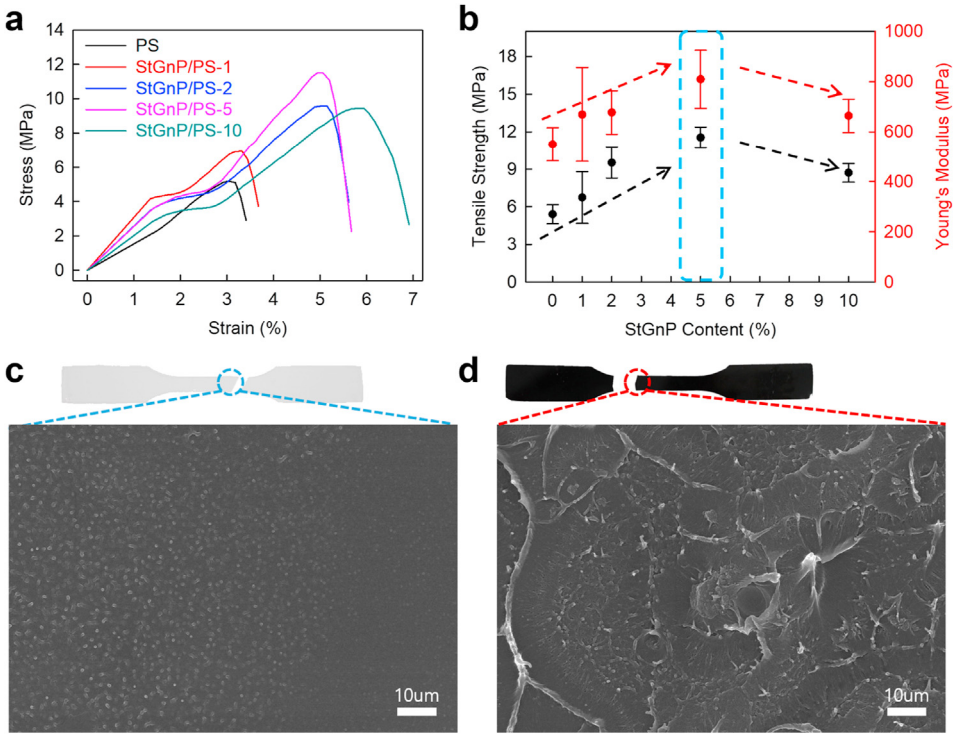

Fig. 3 – (a) Stress–strain curves of pure PS and the StGnP/PS nanocomposites; (b) Tensile strength and Young's modulus of pure PS and the StGnP/PS nanocomposites. SEM images of the fractured surfaces after the tensile test: (c) pure PS and (d) StGnP/PS-5 nanocomposite.

Table 1 – Mechanical properties of pure PS and the StGnP/PS nanocomposites.

	Tensile Strength (MPa)	Young's Modulus (MPa)	Yield Strength (MPa)	Tensile Toughness (MPa)
PS	5.40 ± 0.84	549.2 ± 75.4	2.42 ± 0.45	0.40 ± 0.12
StGnP/PS-1	6.73 ± 2.38	668.9 ± 118.0	2.64 ± 1.48	0.43 ± 0.27
StGnP/PS-2	9.52 ± 1.28	677.3 ± 93.7	2.95 ± 0.54	0.98 ± 0.16
StGnP/PS-5	11.54 ± 0.84	809.4 ± 133.3	3.67 ± 0.52	0.89 ± 0.15
StGnP/PS-10	8.70 ± 0.75	663.7 ± 69.7	2.96 ± 0.27	1.09 ± 0.29

additive for PS. Thus, the StGnPs (when used as a reinforcing additive) improved the mechanical properties of PS due to their good dispersibility in the PS matrix. Moreover, the StGnPs exhibited efficient load transfer and outstanding mechanical properties.

Tensile tests were carried out on solution-cast and molded specimens of pure PS and the StGnP/PS nanocomposites (StGnP loading = 1, 2, 5, and 10 wt.%) (Fig. S8). The stress–strain curves of pure PS and the StGnP/PS nanocomposites are shown in Fig. 3a. The plateau of the StGnP/PS nanocomposites in stress–strain curves are associated with yield point of the pure PS as can be seen in Fig. 3a [51]. The mechanical properties including the tensile strength, Young's modulus, yield strength, and elongation at break of the nanocomposites depended on their StGnP contents. As can be observed from Fig. 3b and Table 1, the tensile strength, Young's modulus, yield strength, and tensile toughness of the StGnP/PS nanocomposites were significantly higher than those of pure PS (5.40, 549.2, 2.42, and 0.40 MPa, respectively). The mechanical properties of the nanocomposites improved with an increase in their StGnP loading. The best mechanical properties were obtained at the StGnP loading of 5 wt.% (Table 1). The StGnP/PS-5 nanocomposite showed the highest tensile strength (11.54 MPa), Young's modulus (809.4 MPa), yield strength (3.67 MPa), and tensile toughness (0.89 MPa) among all the samples. The tensile strength, Young's modulus, yield strength, and tensile toughness of the StGnP/PS-5 nanocomposite were 113.7, 47.4, 51.7, and 122.5% higher than those of pure PS, respectively. In addition, the StGnP/PS-5 nanocomposite showed much higher tensile strength than the GO/PS nanocomposites reported previously (Table S3).

The significantly enhanced mechanical properties of the StGnP/PS nanocomposites as compared to those of pure PS can be attributed to the molecular-level dispersion of the StGnPs in the PS matrix, which resulted in strong interfacial adhesion between PS and the styrene moieties at the edges of the StGnPs with a large SSA. Thus, the applied stress could be efficiently transferred from PS to the StGnPs, which improved the mechanical properties of the nanocomposites. In addition, π-π interactions between StGnPs and PS improved the

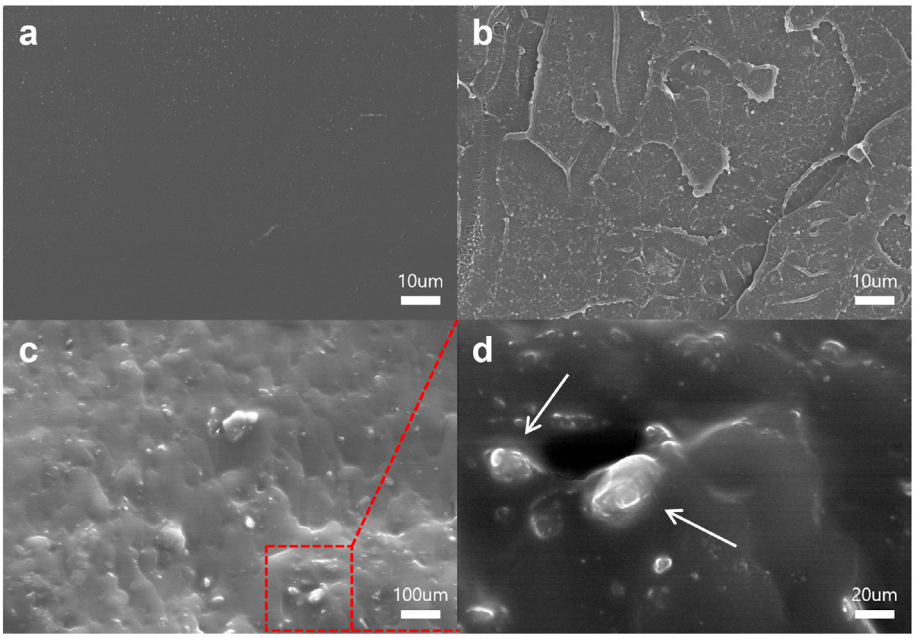

Fig. 4 – SEM images of the cryo-fractured surfaces of the specimens: (a) pure PS and (b) StGnP/PS-5 nanocomposite. SEM images of the fractured StGnP/PS-5 nanocomposite after heat-treatment at 100 °C in N_2: (c) low-magnification; (d) high-magnification.

mechanical properties of nanocomposites. The StGnPs loadings of more than 10 wt.% deteriorated the mechanical properties of the StGnP/PS nanocomposites. This indicates that the maximum compatibility of the StGnPs with the PS matrix was achieved at the StGnP loadings less than 10 wt.%. However, the mechanical properties of the StGnP/PS nanocomposites were superior to those of pure PS even at the StGnPs loadings of more than 10 wt.%. The deterioration of the mechanical properties of the nanocomposites at high StGnP loadings can be attributed to the agglomeration of excess StGnPs in the PS matrix [52]. The tensile toughness (area of the S–S curve, elongation to break) of the StGnP/PS nanocomposites improved with an increase in the StGnP loading because of the sliding effect of the StGnPs with a few layers along the direction of the applied stress (Fig. S9). The mechanical performance results of the StGnP/PS nanocomposites revealed that the StGnPs were uniformly dispersed in the PS matrix and showed strong interaction with it, allowing an efficient load transfer [52,53].

To further investigate the role of the StGnPs in improving the mechanical properties of PS, the morphologies of the fracture surfaces of the StGnP/PS nanocomposites subjected to the tensile tests were examined. The FE-SEM images of the fracture surfaces between pure PS and the StGnP/PS-5 nanocomposites were compared. Pure PS showed a smooth and even fracture surface (Fig. 3c), indicating that the sample failed sharply at low stress after little elongation. In contrast, the StGnP/PS-5 nanocomposite displayed a rough and ravine-like fractured surface (Fig. 3d), indicating that its film broke gradually after the accumulation of stress because of an efficient load transfer from PS to the StGnPs. Therefore, the outstanding mechanical properties of the StGnP/PS nanocomposites can be attributed to the uniform dispersion of the StGnPs in the PS matrix and the strong interaction among them.

The cryo-fractured specimens of the samples were further examined to investigate the relationship between their mechanical properties and morphologies (Figs. 4a, b, and S10). The fractured surface of StGnP/PS-5 (Fig. 4b) was much rougher than that of pure PS (Fig. 4a). In addition, the agglomeration of the StGnPs was not observed (Fig. S10) in the case of the StGnP/PS-5 nanocomposite, indicating that the StGnPs were uniformly dispersed and completely coated with the PS matrix (sky blue arrows in Figs. S10b and S10d). The formation of a rough fracture surface can be attributed to the multi-dimensional structure of the stitched hybrid filler and the comparatively soft polymer chain of the stitching segment, which enhanced the load transfer from the PS matrix to the StGnPs. To further confirm the uniform dispersion of the StGnPs in the PS matrix, the fractured specimen of StGnP/PS-5 was annealed at 100 °C in N_2 and then its SEM images were obtained. As expected, the SEM images showed that the StGnP/PS-5 specimen had a wart-like morphology (Fig. 4c) and the StGnPs were coated heavily with PS (Fig. 4c), confirming the high degree of dispersion of the StGnPs in the PS matrix. The high styrene concentration of the StGnPs significantly improved their affinity to the PS matrix and their dispersibility in it, thus improving the mechanical properties of the nanocomposites.

The thermal stability of the StGnP/PS nanocomposites and pure PS was evaluated by carrying out their TGA in air. The TGA profiles revealed that the StGnPs efficiently improve the thermal stability of pure PS. The degradation temperature ($T_{d10\%}$) at 10 wt.% weight loss of pure PS was 315.4 °C. On the

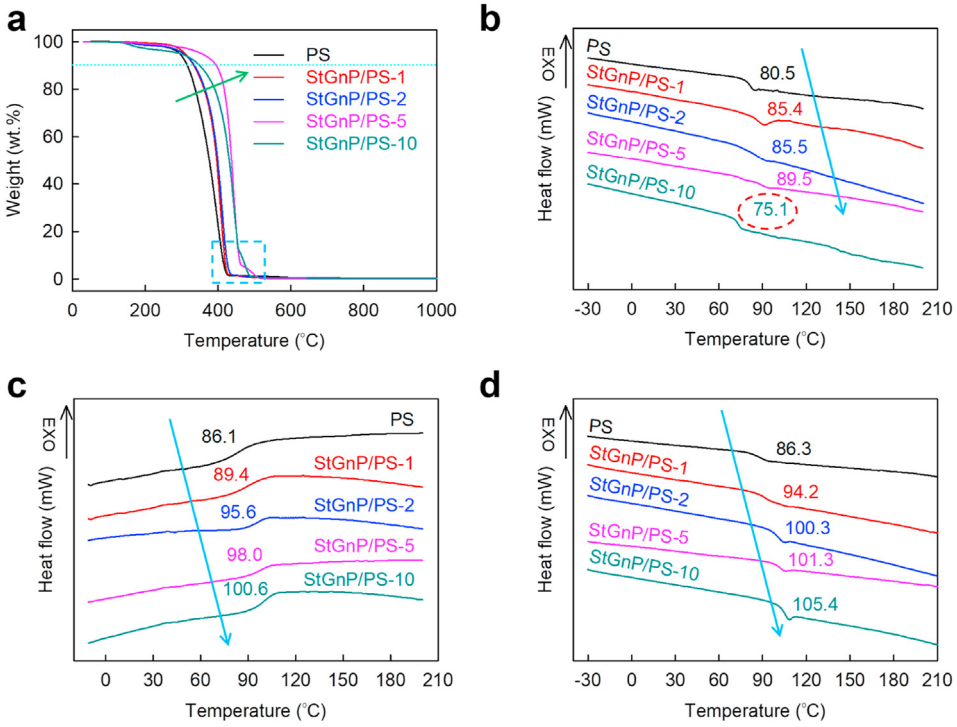

Fig. 5 – (a) TGA curves of pure PS and the StGnP/PS nanocomposites at the heating rate of 10 °C min^{-1} in air. DSC curves of pure PS and the StGnP/PS nanocomposites at the ramping rate of 10 °C min^{-1} in N_2: (b) 1st heating; (c) 1st cooling; (d) 2nd heating.

other hand, the $T_{d10\%}$s of the StGnP/PS nanocomposites with the StGnPs loadings of 1, 2, 5, or 10 wt.% were 332.9, 334.7, 394.7, or 349.1 °C, respectively. The thermal stability of pure PS improved significantly with the incorporation of the StGnPs (Fig. 5a). Among all the nanocomposites, StGnP/PS-5 showed the highest increase in the $T_{d10\%}$ (79.3 °C). The enhanced thermal stability of the StGnP/PS nanocomposites can be attributed to the very high aspect ratio of the well-dispersed StGnPs in the PS matrix, preventing the evolution of small thermally degraded gaseous molecules.

The relaxation behaviors of the functionalization groups grafted to a solid surface (*e.g.*, StGnPs) are distinctively different for free and entangled chains. This unique difference can be used to identify the type of interaction between a polymer and solid additive (filler). The segmental dynamics of polymers is essentially cooperative and is strongly affected by additives. The glass transition temperature (T_g) is a macroscopic indication of the relaxation behavior of nanocomposites, and its magnitude depends on multiple structural parameters. Differential scanning calorimetry (DSC) measurements were carried out to quantify the changes in the T_gs of the samples (Fig. 5b, c, and 5d). The T_g of the StGnP/PS nanocomposites increased significantly with an increase in the StGnP loading because of the strong interaction between the StGnP sheets and PS chains. However, in the first heating scan, only StGnP/PS-10 showed a T_g (75.1 °C) less than that of pure PS (80.5 °C) (Fig. 5b) because of its large free volume (void) due to excess StGnP aggregates [54]. At temperatures higher than 210 °C, the T_g of the samples increased gradually with an increase in the StGnP loading during both the first cooling (Fig. 5c) and second heating scans (Fig. 5d).

4. Conclusions

In summary, we prepared directly StGnPs *via* a mechanochemical reaction between graphite and styrene without additional chemical reaction. The structure of the StGnPs was examined using various analytical techniques, including SEM, FT-IR, EDS, XPS, TGA, and XRD. Especially, the StGnPs showed good dispersibility in common organic solvents (*e.g.*, THF) and high compatibility with PS because of the chemical similarity between the styrene moieties on the StGnPs and PS. StGnP/PS nanocomposites with various StGnP loadings were prepared easily by solution process method. The nanocomposites showed outstanding mechanical properties and thermal stability compared to pure PS. The StGnP/PS nanocomposite with 5 wt.% StGnP loading demonstrated the best mechanical and thermal properties among all the nanocomposites. The tensile strength, Young's modulus, yield strength, and tensile toughness of the StGnP/PS-5 nanocomposite were 113.7, 47.4, 51.7, and 122.5% higher than those pure PS, respectively. The findings of this study suggest that owing to their excellent mechanical and thermal properties and cost-effectiveness GnPs with various functional groups (*e.g.*, styrene in this work) can be used as promising reinforcing additives for various polymers. The results obtained in this study demonstrate the potential of the mechanochemical reaction as an

efficient approach to functionalize the edges of graphitic materials with various target groups for application as reinforcing additives to polymers.

Declaration of Competing Interest

The authors declare that they have no known competing financial interests or personal relationships that could have appeared to influence the work reported in this paper.

Acknowledgements

This research was supported by Wonkwang University in 2019.

Appendix A. Supplementary data

Supplementary data to this article can be found online at https://doi.org/10.1016/j.jmrt.2020.12.039.

REFERENCES

[1] Jeon I-Y, Noh H-J, Baek J-B. Nitrogen-Doped carbon nanomaterials: synthesis, characteristics and applications. Chem Asian J 2020;15(15):2282–93.
[2] Wehling TO, Novoselov KS, Morozov SV, Vdovin EE, Katsnelson MI, Geim AK, et al. Molecular doping of graphene. Nano Lett 2008;8(1):173–7.
[3] Wang X, Sun G, Routh P, Kim D-H, Huang W, Chen P. Heteroatom-doped graphene materials: syntheses, properties and applications. Chem Soc Rev 2014;43(20):7067–98.
[4] Fasolino A, Los JH, Katsnelson MI. Intrinsic ripples in graphene. Nat Mater 2007;6(11):858–61.
[5] Pokharel P, Bae H, Lim J-G, Lee KY, Choi S. Effects of titanate treatment on morphology and mechanical properties of graphene nanoplatelets/high density polyethylene nanocomposites. J Appl Polym Sci 2015;132(23) [n/a-n/a].
[6] Iqbal MZ, Abdala AA, Mittal V, Seifert S, Herring AM, Liberatore MW. Processable conductive graphene/polyethylene nanocomposites: effects of graphene dispersion and polyethylene blending with oxidized polyethylene on rheology and microstructure. Polymer 2016;98:143–55.
[7] Song HD, Im Y-K. Baek, J-B, Jeon, I-Y, Heptene-functionalized graphitic nanoplatelets for high performance composites of linear low-density polyethylene. Compos Sci Technol 2020;199:108380.
[8] Song P, Cao Z, Cai Y, Zhao L, Fang Z, Fu S. Fabrication of exfoliated graphene-based polypropylene nanocomposites with enhanced mechanical and thermal properties. Polymer 2011;52(18):4001–10.
[9] Bafana AP, Yan X, Wei X, Patel M, Guo Z, Wei S, et al. Polypropylene nanocomposites reinforced with low weight percent graphene nanoplatelets. Composites Part B 2017;109:101–7.
[10] Sánchez-Valdes S, Zapata-Domínguez AG, Martinez-Colunga JG, Mendez-Nonell J, Ramos de Valle LF, Espinoza-Martinez AB, et al. Influence of functionalized polypropylene on polypropylene/graphene oxide nanocomposite properties. Polym Compos 2016;39(4):1361–9.
[11] Zhao Y, Lu J, Liu X, Wang Y, Lin J, Peng N, et al. Performance enhancement of polyvinyl chloride ultrafiltration membrane modified with graphene oxide. J Colloid Interface Sci 2016;480:1–8.
[12] Amanzadeh H, Yamini Y, Moradi M, Asl YA. Determination of phthalate esters in drinking water and edible vegetable oil samples by headspace solid phase microextraction using graphene/polyvinylchloride nanocomposite coated fiber coupled to gas chromatography-flame ionization detector. J Chromatogr A 2016;1465:38–46.
[13] Tu Z, Wang J, Yu C, Xiao H, Jiang T, Yang Y, et al. A facile approach for preparation of polystyrene/graphene nanocomposites with ultra-low percolation threshold through an electrostatic assembly process,. Compos Sci Technol 2016;134:49–56.
[14] Ai Y, Hsu TH, Wu DC, Lee L, Chen J-H, Chen Y-Z, et al. An ultrasensitive flexible pressure sensor for multimodal wearable electronic skins based on large-scale polystyrene ball@reduced graphene-oxide core–shell nanoparticles. J Mater Chem C 2018;6(20):5514–20.
[15] Yu Y-H, Lin Y-Y, Lin C-H, Chan C-C, Huang Y-C. High-performance polystyrene/graphene-based nanocomposites with excellent anti-corrosion properties. Polym Chem 2014;5(2):535–50.
[16] Wang G, Dai Z, Liu L, Hu H, Dai Q, Zhang Z. Tuning the interfacial mechanical behaviors of monolayer graphene/PMMA nanocomposites. ACS Appl Mater Interfaces 2016;8(34):22554–62.
[17] Borin Barin G, Song Y, de Fátima Gimenez I, Souza Filho AG, Barreto LS, Kong J. Optimized graphene transfer: influence of polymethylmethacrylate (PMMA) layer concentration and baking time on graphene final performance. Carbon 2015;84:82–90.
[18] Tung TT, Robert C, Castro M, Feller JF, Kim TY, Suh KS. Enhancing the sensitivity of graphene/polyurethane nanocomposite flexible piezo-resistive pressure sensors with magnetite nano-spacers. Carbon 2016;108:450–60.
[19] Liu H, Huang W, Yang X, Dai K, Zheng G, Liu C, et al. Organic vapor sensing behaviors of conductive thermoplastic polyurethane–graphene nanocomposites. J Mater Chem C 2016;4(20):4459–69.
[20] Zhang S, Shen X, Zheng Z, Ma Y, Qu Y. 3D graphene/nylon rope as a skeleton for noble metal nanocatalysts for highly efficient heterogeneous continuous-flow reactions. J Mater Chem A 2015;3(19):10504–11.
[21] Gong L, Yin B. Li L-p, Yang M-b, Nylon-6/Graphene composites modified through polymeric modification of graphene. Composites Part B 2015;73:49–56.
[22] Song SH, Park KH, Kim BH, Choi YW, Jun GH, Lee DJ, et al. Enhanced thermal conductivity of epoxy–graphene composites by using non-oxidized graphene flakes with non-covalent functionalization, adv. Mater 2013;25(5):732–7.
[23] Lerf A, He H, Forster M, Klinowski J. Structure of graphite oxide revisited‖. J Phys Chem B 1998;102(23):4477–82.
[24] Gómez-Navarro C, Meyer JC, Sundaram RS, Chuvilin A, Kurasch S, Burghard M, et al. Atomic structure of reduced graphene oxide. Nano Lett 2010;10(4):1144–8.
[25] Cai W, Piner RD, Stadermann FJ, Park S, Shaibat MA, Ishii Y, et al. Synthesis and solid-state NMR structural characterization of ^{13}C-labeled graphite oxide. Science 2008;321(5897):1815–7.
[26] Tan B, Thomas NL. A review of the water barrier properties of polymer/clay and polymer/graphene nanocomposites,. J Membr Sci 2016;514:595–612.
[27] Ji X, Xu Y, Zhang W, Cui L, Liu J. Review of functionalization, structure and properties of graphene/polymer composite fibers. Composites Part A 2016;87:29–45.

[28] Balazs AC, Emrick T, Russell TP. Nanoparticle polymer composites: where two small worlds meet. Science 2006;314(5802):1107–10.
[29] Punetha VD, Rana S, Yoo HJ, Chaurasia A, McLeskey JT, Ramasamy MS, et al. Functionalization of carbon nanomaterials for advanced polymer nanocomposites: a comparison study between CNT and graphene,. Prog Polym Sci 2017;67:1–47.
[30] Choudhary S, Mungse HP, Khatri OP. Dispersion of alkylated graphene in organic solvents and its potential for lubrication applications. J Mater Chem 2012;22(39):21032.
[31] Tessonnier J-P, Barteau MA. Dispersion of alkyl-chain-functionalized reduced graphene oxide sheets in nonpolar solvents. Langmuir 2012;28(16):6691–7.
[32] Edge-carboxylated graphene nanosheets via ball millingJeon IY, Shin YR, Sohn GJ, Choi HJ, Bae SY, Mahmood J, et al., editors. Proc Natl Acad Sci US.A 2012;109(15):5588–93.
[33] Jeon I-Y, Choi H-J, Jung S-M, Seo J-M, Kim M-J, Dai L, et al. Large-Scale production of edge-selectively functionalized graphene nanoplatelets via ball milling and their use as metal-free electrocatalysts for oxygen reduction reaction. J Am Chem Soc 2012;135(4):1386–93.
[34] Jeon I-Y, Choi M, Choi H-J, Jung S-M, Kim M-J, Seo J-M, et al. Baek J-B antimony-doped graphene nanoplatelets, nat. Commun Now 2015;6:7123.
[35] Fastyn P, Kornacki W, Gierczak T, Gawłowski J, Niedzielski J. Adsorption of water vapour from humid air by selected carbon adsorbents. J Chromatogr A 2005;1078(1–2):7–12.
[36] Jeon I-Y, Choi H-J, Choi M, Seo J-M, Jung S-M, Kim M-J, et al. Facile, scalable synthesis of edge-halogenated graphene nanoplatelets as efficient metal-free eletrocatalysts for oxygen reduction reaction, Sci. For Rep 2013;(1):3.
[37] Stankovich S, Piner RD, Nguyen ST, Ruoff RS. Synthesis and exfoliation of isocyanate-treated graphene oxide nanoplatelets. Carbon 2006;44(15):3342–7.
[38] Jeon I-Y, Choi M, Choi H-J, Jung S-M, Kim M-J, Seo J-M, et al. Antimony-doped graphene nanoplatelets. Nat Commun 2015;(1):6.
[39] Sohn G-J, Choi H-J, Jeon I-Y, Chang DW, Dai L, Baek J-B. Water-dispersible, sulfonated hyperbranched poly(ether-ketone) grafted multiwalled carbon nanotubes as oxygen reduction catalysts. ACS Nano 2012;6(7):6345–55.
[40] Idibie CA, Abdulkareem SA. Pienaar CHv, iyuke SE, vanDyk L, mechanism and kinetics of sulfonation of Polystyrene–Butadiene rubber with chlorosulfonic acid. Ind Eng Chem Res 2010;49(4):1600–4.
[41] Allouche A, Ferro Y. Dissociative adsorption of small molecules at vacancies on the graphite (0001) surface. Carbon 2006;44(15):3320–7.
[42] Lesiak B, Kövér L, Tóth J, Zemek J, Jiricek P, Kromka A, et al. C sp2/sp3 hybridisations in carbon nanomaterials – XPS and (X)AES study. Appl Surf Sci 2018;452:223–31.
[43] Stobinski L, Lesiak B, Malolepszy A, Mazurkiewicz M, Mierzwa B, Zemek J, et al. Graphene oxide and reduced graphene oxide studied by the XRD, TEM and electron spectroscopy methods, J. Electron. Spectrosc. Relat. Phenom 2014;195:145–54.
[44] Stoller MD, Park S, Zhu Y, An J, Ruoff RS. Graphene-based ultracapacitors. Nano Lett 2008;8(10):3498–502.
[45] Thommes M. Physical adsorption characterization of nanoporous materials. Chem Ing Tech 2010;82(7):1059–73.
[46] Jeon I-Y, Yu D, Bae S-Y, Choi H-J, Chang DW, Dai L, et al. formation of large-area nitrogen-doped graphene film prepared from simple solution casting of edge-selectively functionalized graphite and its electrocatalytic activity, chem. Mater 2011;23(17):3987–92.
[47] Inagaki M, Fujita K, Takeuchi Y, Oshida K, Iwata H, Konno H. Formation of graphite crystals at 1000–1200°C from mixtures of vinyl polymers with metal oxides. Carbon 2001;39(6):921–9.
[48] Seidl L, Bucher N, Chu E, Hartung S, Martens S, Schneider O, et al. Intercalation of solvated Na-ions into graphite. Energy Environ Sci 2017;10(7):1631–42.
[49] Maul J, Frushour BG, Kontoff JR, Eichenauer H, Ott K-H, Schade C, et al, Ullmann's encyclopedia of industrial chemistry, wiley-VCH verlag GmbH & Co. KGaA2007.
[50] Zhang Z, Han Y, Li T, Wang T, Gao X, Liang Q, et al. Polyaniline/montmorillonite nanocomposites as an effective flame retardant and smoke suppressant for polystyrene. Synth Met 2016;221:28–38.
[51] Faridmehr I, Osman MH, Adnan AB, Nejad AF, Hodjati R, Azimi M. Correlation between engineering stress-strain and true stress-strain curve, Am. J Civ Eng 2014;2(1):53–9.
[52] Tang L-C, Wang X, Gong L-X, Peng K, Zhao L. Chen, Q, Wu L-B, Jiang J-X, Lai G-Q Creep and recovery of polystyrene composites filled with graphene additives. Compos Sci Technol 2014;91:63–70.
[53] Yang S-Y, Lin W-N, Huang Y-L, Tien H-W, Wang J-Y, Ma C-CM, et al. Synergetic effects of graphene platelets and carbon nanotubes on the mechanical and thermal properties of epoxy composites. Carbon 2011;49(3):793–803.
[54] Tong J, Huang H-X, Wu M. Promoting compatibilization effect of graphene oxide on immiscible PS/PVDF blend via water-assisted mixing extrusion. Compos Sci Technol 2017;149:286–93.